iScience

CellPress
OPEN ACCESS

Article

StemRegenin 1 attenuates the RANKL-induced osteoclastogenesis via inhibiting AhR-c-src-NF-κB/p-ERK MAPK-NFATc1 signaling pathway

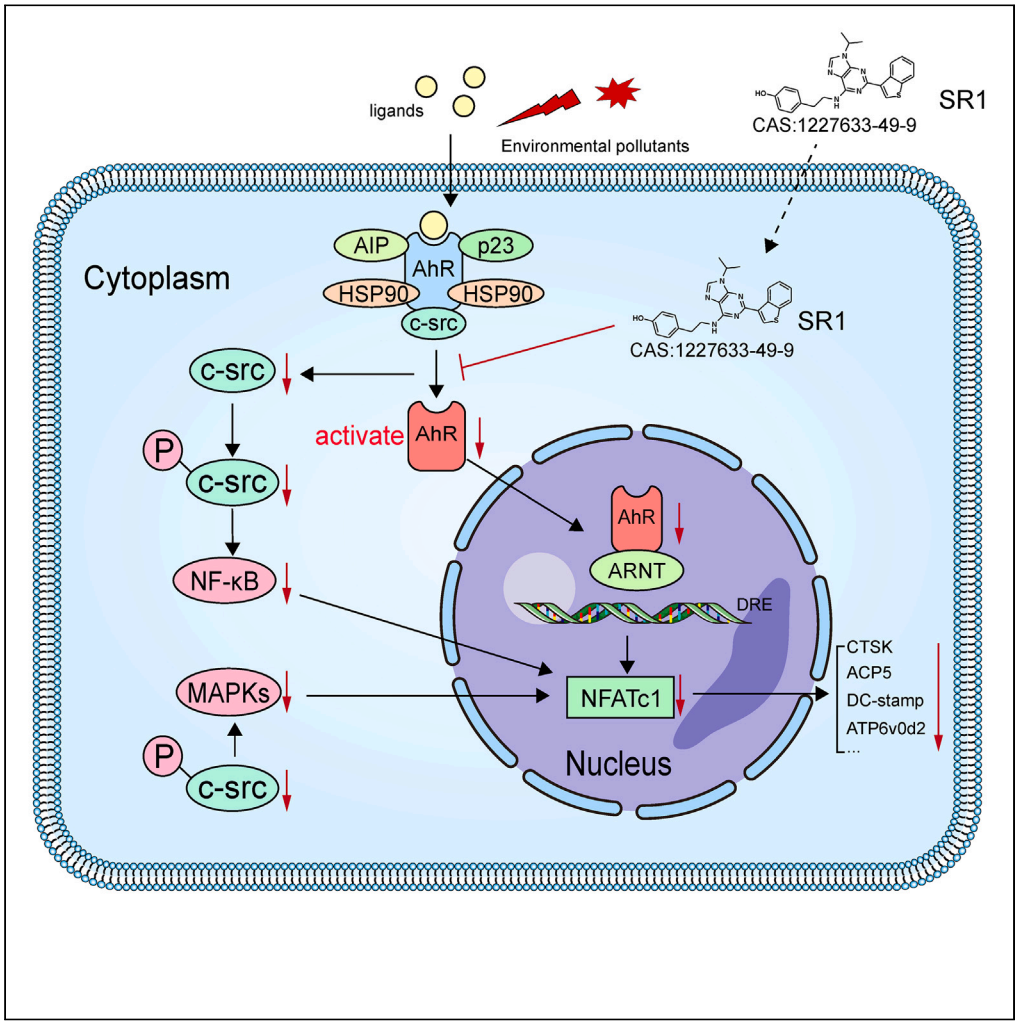

Shengji Zhou, Jiarui Li, Tiantian Ying, Yuxin Wang, Quan Wang, Xiang Li, Fengchao Zhao

idea_lixiang@zju.edu.cn (X.L.)
zhaofengchao@zju.edu.cn (F.Z.)

Highlights

SR1 can inhibit RANKL-induced osteoclastogenesis

SR1 inhibits osteoclasts differentiation mainly by inhibiting AhR in the early stage

SR1 attenuates osteoclastogenesis via inhibiting AhR-c-src-NF-κB/p-ERK MAPK

SR1 significantly improved bone loss in OVX mice *in vivo*

Zhou et al., iScience 27, 109682
May 17, 2024
https://doi.org/10.1016/j.isci.2024.109682

iScience

CellPress
OPEN ACCESS

Article

StemRegenin 1 attenuates the RANKL-induced osteoclastogenesis via inhibiting AhR-*c*-src-NF-κB/p-ERK MAPK-NFATc1 signaling pathway

Shengji Zhou,[1,2] Jiarui Li,[1,2] Tiantian Ying,[1,2] Yuxin Wang,[1] Quan Wang,[1] Xiang Li,[1,*] and Fengchao Zhao[1,3,*]

SUMMARY

The aryl hydrocarbon receptor (AhR) pathway may play an important role in the regulation of osteoclasts, but there are still conflicting studies on this aspect, and the specific mechanism of action has not been fully elucidated. Therefore, we conducted this study to find a drug to treat osteoporosis that targets AhR. We found that StemRegenin 1 inhibited RANKL-induced osteoclastogenesis in a concentration-dependent and time-dependent manner. Through further experiments, we found that SR1 can inhibit nuclear transcription of AhR and inhibit c-src phosphorylation, and ultimately regulates the activation of the NF-κB and *p*-ERK/mitogen-activated protein kinase pathways. Therefore, for the first time, we discovered the way in which the AhR-*c*-src-NF-κB/p-ERK MAPK-NFATc1 signaling pathway regulates the expression of osteoclast differentiation-associated proteins. Finally, SR1 was shown to successfully reverse bone loss in OVX mice. These studies provide us with ideas for finding new way to treat osteoporosis.

INTRODUCTION

Statistically, fractures due to osteoporosis are becoming more common in women after the age of 55, leading to a large number of bone-related diseases and increasing mortality and health care costs.[1] Bone metabolism is a dynamic process, and the dynamic activities of bone formation and reabsorption reaches a balance in normal physiological activities. However, in case of bone loss, the balance established by osteoclasts and osteoblasts is broken.[2] Due to the decrease of ovarian estrogen secretion after menopause, it will lead to increased bone resorption and a relative decrease in bone formation. As the only cell with bone resorption function in the body, the regulation of osteoclasts differentiation is extremely important for alleviating the development of postmenopausal bone shortening.[3]

Osteoclasts are derived from monocyte/macrophage hematopoietic progenitor cells.[4] Osteoclasts are nonspecifically dependent on macrophage proliferation and survival cytokine macrophage colony stimulating factor (M-CSF) in the early stages of differentiation, followed by receptor activator of nuclear factor-kappa B ligand (RANKL) expressed by osteoblasts to activate RANK to differentiate into osteoclasts.[5] After menopause, the deficiency of estrogen (E2) causes circulating monocytes to release interleukin-1 (IL-1) and tumor necrosis factor-α (TNF-α), which are involved in bone resorbtion and lead to increased osteoclasts.[6] Meanwhile, T cells secrete a large amount of RANKL, bind to its receptor rank, recruit TRAF, and activate the signaling pathway downstream of TNF receptor-associated factor (TRAF). And nuclear factor-kappa B (NF-κB) and mitogen activated protein kinases (MAPKs) activated the nuclear factor of T cell 1 (NFATc1), which is an important regulator of osteoclasts differentiation. NFATc1 can directly affect osteoclasts differentiation and expression of osteoclast-related genes, such as tartrate-resistant acid-base phosphatase (TRAP) and cathepsin K (CTSK) and dendritic cell-specific transmembrane protein (DC-STAMP).[7,8] Finally, NFATc1 can promote the formation of osteoclasts. Alternatively, RANKL may promote the expression of NFATc1 by inducing c-Fos and AP-1 activation, thus promoting the production of osteoclasts.[9] In addition, experiments have shown that the formation of osteoclasts in mice knocked out by NFATc1 is severely hindered, and the expression of osteoclast differentiation-associated genes is also significantly inhibited.[10]

Aryl hydrocarbon receptor (AhR) is a ligand-activated transcription factor of the Pern-Arnt-Sim (PAS) superfamily. AhR is known to be involved in the progression of inflammatory and immune diseases by regulating Th17 and regulatory T cell differentiation.[11] Recent studies have also clarified that AhR plays an important role in bone remodeling.[12] In the unstimulated state, AhR interacts with helper p23, AhR interacting protein (XAP2), nonreceptor tyrosine kinase (c-src) and heat shock protein (Hsp90) in the cytoplasm and forms a stable protein complex. After binding AhR to its ligand, AhR is dissociated from the protein complex,[13] transported to the nucleus, interacts with the aromatics receptor nuclear transporter (ARNT), and binds to the dioxin reaction element (DRE) sequence. Thus, the expression of cytochrome P450 subfamily B member 1 (CYP1B1), aryl hydrocarbon receptor repressor (AHRR) and other downstream genes were induced.[14] As an inhibitor of the AhR signaling pathway, StemRegenin 1 (SR1) has been shown to improve the expansion of human primordial hematopoietic stem cells under

[1]Department of Orthopaedic Surgery, The First Affiliated Hospital, Zhejiang University School of Medicine, Hangzhou 310003, P.R. China
[2]These authors contributed equally
[3]Lead contact
*Correspondence: idea_lixiang@zju.edu.cn (X.L.), zhaofengchao@zju.edu.cn (F.Z.)
https://doi.org/10.1016/j.isci.2024.109682

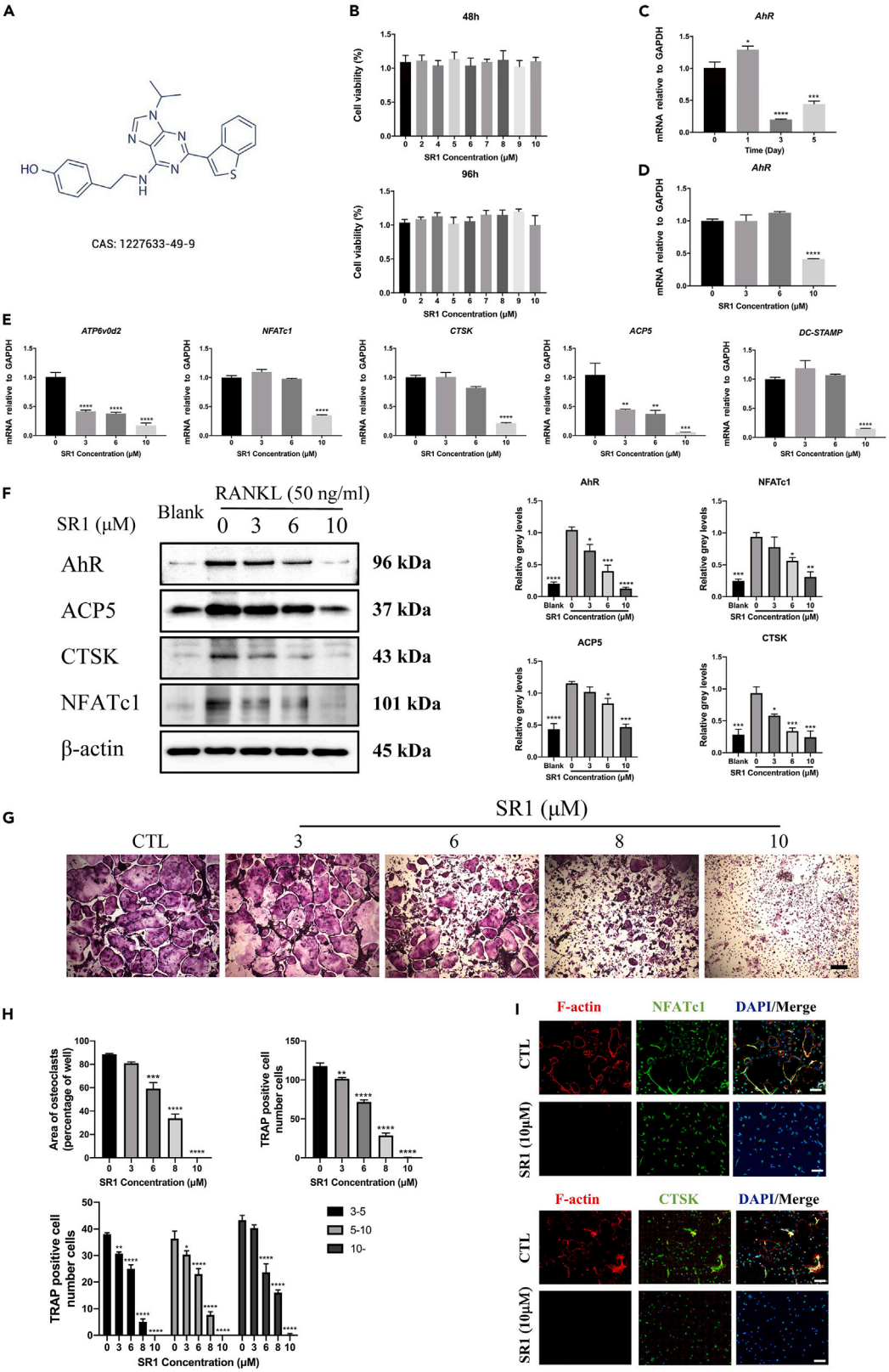
A
HO
N
N
N
N
H
S
CAS: 1227633-49-9
B
48h
96h
Cell viability (%)
SR1 Concentration (μM)
C
AhR
mRNA relative to GAPDH
Time (Day)
D
AhR
mRNA relative to GAPDH
SR1 Concentration (μM)
E
ATP6v0d2
NFATc1
CTSK
ACP5
DC-STAMP
mRNA relative to GAPDH
SR1 Concentration (μM)
F
SR1 (μM)
Blank
RANKL (50 ng/ml)
0 3 6 10
AhR
ACP5
CTSK
NFATc1
β-actin
96 kDa
37 kDa
43 kDa
101 kDa
45 kDa
Relative grey levels
SR1 Concentration (μM)
G
SR1 (μM)
CTL
3
6
8
10
H
Area of osteoclasts (percentage of well)
TRAP positive cell number cells
SR1 Concentration (μM)
3-5
5-10
10-
I
F-actin
NFATc1
DAPI/Merge
CTL
SR1 (10μM)
F-actin
CTSK
DAPI/Merge
CTL
SR1 (10μM)

Figure 1. SR1 inhibits RANKL-induced osteoclastogenesis in a concentration-dependent manner

(A) The chemical structural formula of StemRegenin 1.

(B) The cell viability of different concentration gradients SR1-stimulated BMMs after 48 h and 96 h.

(C) The BMMs were induced by 25 ng/mL MCSF and 50 ng/mL RANKL for indicated periods, the mRNA expression levels of AhR was detected by qPCR.

(D) The BMMs were induced by 25 ng/mL MCSF and 50 ng/mL RANKL and stimulated with SR1 at indicated concentrations for 4 days, the mRNA expression levels of AhR was detected by qPCR.

(E) The BMMs were induced by 25 ng/mL MCSF and 50 ng/mL RANKL and stimulated with SR1 at indicated concentrations for 4 days, the mRNA expression levels of osteoclasts-specific genes, including NFATc1, ACP5, DC-STAMP, ATP6v0d2, CTSK, were detected by qPCR, and normalized relative to GAPDH.

(F) The BMMs were induced by 25 ng/mL MCSF and 50 ng/mL RANKL and stimulated with SR1 at indicated concentrations for 4 days. Then the western blot was used to show protein expression levels of NFATc1, CTSK, ACP5, and AhR. And quantitative analysis of protein expression levels, normalized to β-actin.

(G) BMMs were induced by 25 ng/mL MCSF and 50 ng/mL RANKL, and stimulated with SR1 at indicated concentrations (3, 6, 8, 10 μM) for 7 days. Osteoclasts formation results were shown using TRAP staining, scale bar, 100 μm.

(H) Quantitative results of multi-nuclear TRAP-positive cell numbers and the area occupied. We divided the multi-nuclear TRAP-positive cells into three groups (3–5, 5–10, and 10-) according to the number of nuclei, and the TRAP-positive cells number of each group was analyzed.

(I) The BMMs were stimulated with 10 μM SR1. The detection of the NFATc1 and CTSK expression level carried out immunofluorescence, Scale bar, 100 μm. Data were presented as means ± SEM; $n = 3$; *$p < 0.05$, **$p < 0.01$, ***$p < 0.001$, ****$p < 0.0001$.

certain conditions.[15–18] In addition, SR1 has the potential ability to promote human plasmacytoid and myeloid dendritic cell development from hematopoietic progenitor cells.[19] It has also been reported that SR1 can promote the terminal differentiation of human erythroblasts and attenuates endothelial progenitor cell senescence by inhibiting AhR signaling.[20,21] Recent studies have shown that the expression of the AhR pathway is associated with bone loss in mice, but various studies have contradicted each other and the specific mechanism of action has not been clarified.[22–24]

In our study, we focused on exploring the role of SR1 in osteoclast formation and osteoblast formation. For the first time, we reveal the AhR-*c*-src-NF-κB/p-ERK MAPK-NFATc1 signaling axis in osteoclasts and confirm the important role of SR1 in ameliorating osteoporosis. This gives us new ideas for trying to find more effective drugs to treat osteoporosis.

RESULTS

SR1 inhibits RANKL-induced osteoclastogenesis in a concentration-dependent manner

The chemical structure formula of SR1 is shown in the figure (Figure 1A), and we verified that the primary cells we used were bone marrow macrophages (BMMs) (Figure S1A). The cytotoxicity of SR1 on BMM cells was determined by 48 h and 96 h CCK8 cytotoxicity assay. The results showed that SR1 had no effect on the proliferative activity of BMMs when the concentration of SR1 was 10 μM or less (Figure 1B). Moreover, through qPCR results, we found that the expression of AhR was significantly increased in the early stage of osteoclast differentiation induced with RANKL (Figure 1C). Previous studies have shown that the stimulation of osteoclasts in the early stage had a more significant impact on their morphology and function.[25,26] Therefore, we suspect that AhR plays an important role in the early differentiation of osteoclasts. Therefore, we selected SR1, a specific inhibitor of AhR, and confirmed that SR1 can effectively reduce the expression of AhR in BMM cells when the BMMs were induced by 25 ng/mL MCSF and 50 ng/mL RANKL and stimulated with SR1 at indicated concentrations for four days (Figure 1D). It was found that when BMMs cells were cultured with the indicated concentrations SR1 for four days, the expression of osteoclast differentiation-associated genes (ACP5, NFATc1, CTSK, DC-STAMP, and ATP6v0d2) decreased with the increase of SR1 concentration (Figure 1E). In addition, at the protein expression level, we also verified that the expression of AhR and osteoclast differentiation-associated proteins (ACP5, CTSK, and NFTAc1) also decreased with the increase of SR1 concentration (Figure 1F). To understand the morphological role of AhR expression changes in osteoclasts formation, we selected an AhR agonist, Norisoboldine, we also first performed CCK8 cytotoxicity assay at 48 h and 96 h, respectively, to determine the toxicity of Norisoboldine on BMMs cells (Figure S2C). We used the indicated concentrations Norisoboldine and SR1 to stimulate BMMs, and observed the number and area of osteoclasts with TRAP staining for the indicated time. It was found that the number and area of osteoclasts could be significantly reduced after AhR was inhibited. In line with this, the number and area of osteoclasts increased after AhR was activated (Figures S2D, S2E, 1G, and 1H). To verify the necessary role of AhR in osteoclast differentiation, we used siAhR to knock down the AhR of BMMs, and found that the expression of osteoclast differentiation-associated proteins was decreased (Figures S1B, S2A, and S2B). At the same time, TRAP staining demonstrated that osteoclast formation was also inhibited when AhR expression was knocked down (Figures S1C and S1D). Moreover, we also confirmed by immunofluorescence experiments that the expression of NFATc1 and CTSK and the formation of F-actin rings in osteoclasts were significantly inhibited under the treatment of 10 μM SR1 (Figure 1I). In conclusion, during the normal differentiation of osteoclasts, inhibition of AhR expression will always result in the low expression of osteoclast differentiation-associated genes and proteins, and within the concentration range of cytotoxic tolerance, the expression levels of AhR and osteoclast-related genes and proteins decrease with the increase of SR1 concentration.

SR 1 inhibits RANKL-induced osteoclastogenesis in a time-dependent manner

We have demonstrated that the expression levels of osteoclast differentiation-associated genes and proteins are inhibited in a concentration-dependent manner by SR1 in the range of cytotoxicity tolerance, but we have not yet confirmed whether the duration of SR1 continuous action has any effect on the expression of osteoclast differentiation-associated gene and proteins. According to previous experiments, we selected 10 μM SR1 as the stimulation concentration to stimulate osteoclast differentiation of BMM cells for 0, 1, 3, and 5 days, respectively. We found

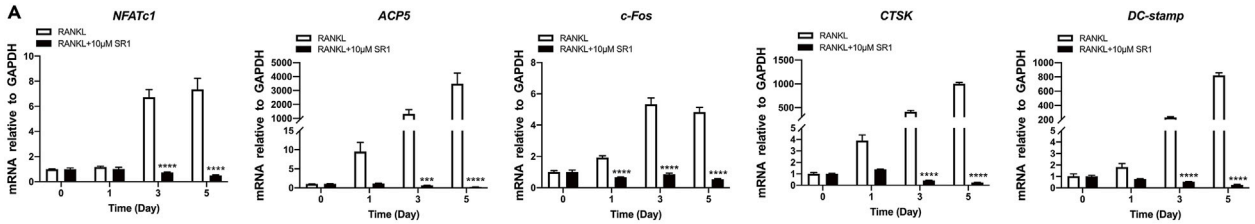
A
NFATc1
ACP5
c-Fos
CTSK
DC-stamp
RANKL
RANKL+10μM SR1
mRNA relative to GAPDH
Time (Day)

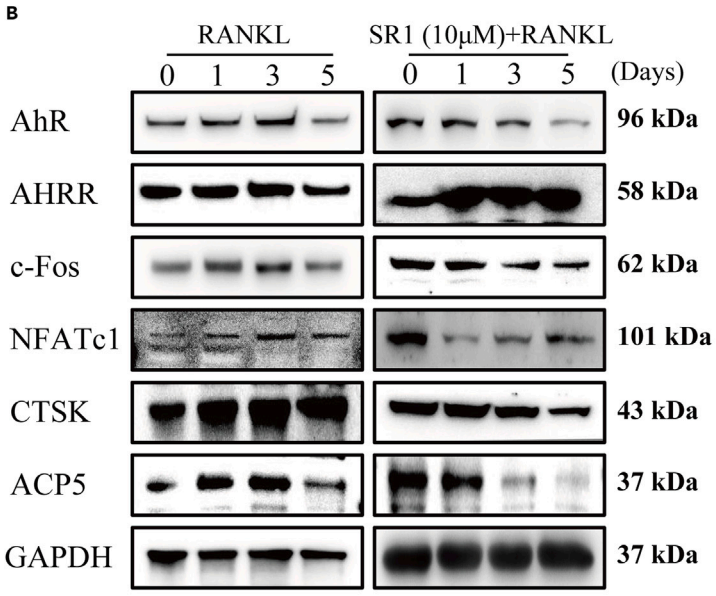
B
RANKL
SR1 (10μM)+RANKL
0 1 3 5 0 1 3 5 (Days)
AhR
AHRR
c-Fos
NFATc1
CTSK
ACP5
GAPDH
96 kDa
58 kDa
62 kDa
101 kDa
43 kDa
37 kDa
37 kDa

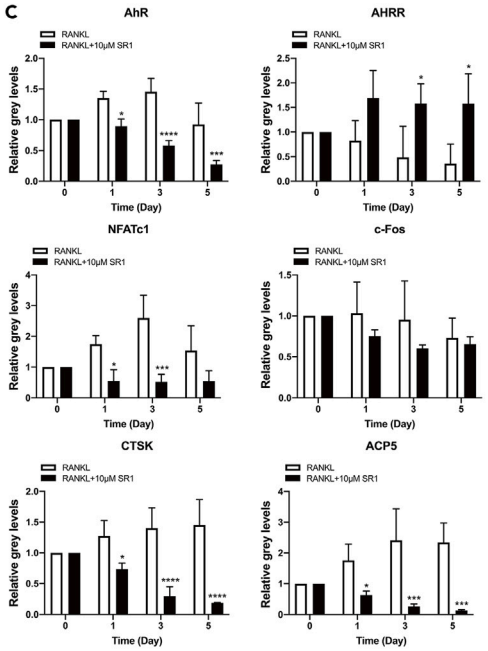
C
AhR
AHRR
NFATc1
c-Fos
CTSK
ACP5
RANKL
RANKL+10μM SR1
Relative grey levels
Time (Day)

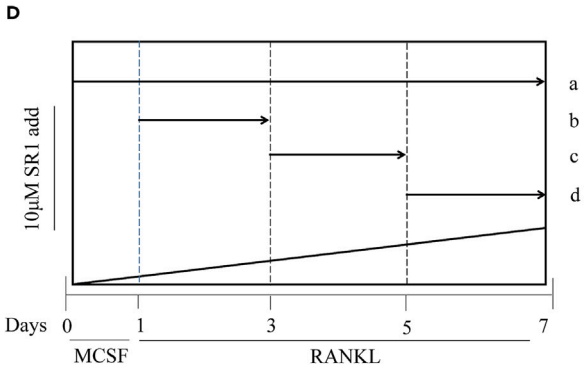
D
10μM SR1 add
a
b
c
d
Days 0 1 3 5 7
MCSF
RANKL

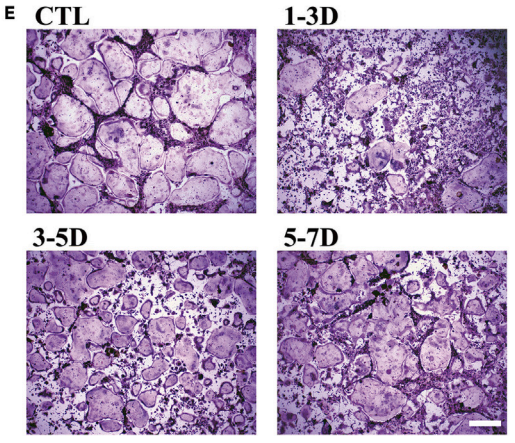
E
CTL
1-3D
3-5D
5-7D

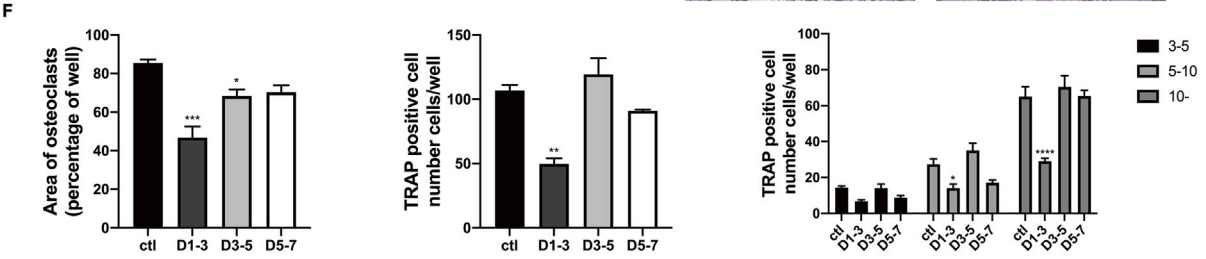
F
Area of osteoclasts (percentage of well)
TRAP positive cell number cells/well
TRAP positive cell number cells/well
ctl
D1-3
D3-5
D5-7
3-5
5-10
10-

Figure 2. SR 1 inhibits RANKL-induced osteoclastogenesis in a time-dependent manner

(A) For 0, 1, 3, 5 days with or without 10 μM of SR1, the treatment of BMMs was carried out with RANKL, and the osteoclastogenesis related genes expression level was detected by qPCR.

(B and C) TFor 0, 1, 3, 5 days with or without 10 μM of SR1, the treatment of BMMs was carried out with RANKL, and Western blot was used to show protein expression levels of NFATc1, CTSK, ACP5, c-Fos, AHRR, and AhR. And quantitative analysis of protein expression levels, normalized to GAPDH.

(D) Patterns of BMMs stimulated with SR1 at different times during the 7 days of BMMs differentiation.

(E and F) BMMs were induced by 25 ng/mL MCSF and 50 ng/mL RANKL, and stimulated with 10 μM SR1 at different stages (1–3, 3–5, 5–7 Day). Quantitative results of multi-nuclear TRAP-positive cell numbers and the area occupied, Scale bar, 100 μm. Data were presented as means ± SEM; $n = 3$; *$p < 0.05$, **$p < 0.01$, ***$p < 0.001$, ****$p < 0.0001$.

that compared with the group stimulated by RANKL, the expression level of osteoclast differentiation-associated gene in the group stimulated by SR1 for the same time showed a downward trend, and this downward trend became more obvious with the extension of SR1 treatment time (Figure 2A). At the same time, we found that after treatment with SR1 for a specified time, the expression levels of AhR and osteoclast differentiation-associated proteins decreased compared with the normal group. With the extension of SR1 treatment time, this downward trend was more obvious. Here, we also detected the expression of AHRR protein during osteoclast differentiation, and found that the expression of AHRR protein increased with the extension of SR1 stimulation time (Figures 2B and 2C). Therefore, we speculated that the high concentrations of SR1 inhibited the expression of AhR by inducing the increase of AHRR expression level, and finally inhibited the osteoclast differentiation-associated gene and protein. In the previous experimental Figure 1C, we speculated that the change of AhR expression in the early stage of osteoclast differentiation would affect the differentiation of osteoclasts. To test this hypothesis, we stimulated the differentiation of BMMs with 10 μM SR1 at the early, middle, and late stages of osteoclasts differentiation (1–3, 3–5, 5–7 Day), and stained osteoclasts with TRAP staining on the 7th day (Figure 2D). We were surprised to find that the inhibition of AhR in the early stage of osteoclasts differentiation (1–3 Day) had the greatest effect on the inhibition of osteoclasts differentiation (Figures 2E, 2F, S1E, and S1F). In conclusion, the high concentrations of SR1 may inhibit the expression of AhR by inducing the expression of AHRR, thus presenting a time-dependent inhibitory effect on osteoclasts differentiation.

SR 1 attenuates the RANKL-induced osteoclastogenesis via inhibiting AhR-*c*-src-NF-κB/p-ERK MAPK signaling pathway

To explore the specific mechanism through which SR1 regulates the occurrence of osteoclasts, we demonstrated by immunofluorescence experiment that compared with the control group that 3 μM SR1 could inhibit the formation of F-actin ring in osteoclasts. 6 μM SR1 could not only inhibit the formation of F-actin ring in osteoclasts, but also prevent AhR from entering the nucleus to play a role. And 10 μM SR1 completely inhibited the formation of F-actin rings and AhR expression in osteoclasts (Figure 3A). We know that c-src is a component of the AhR complex that is stable in the cytoplasm. Moreover, p-*c*-src formed by c-src phosphorylation can play the role of protein kinase.[27] Therefore, we hypothesized that the low concentration of SR1 treatment of BMMs would affect c-src phosphorylation in BMMs. To test our hypothesis, we found that when BMMs were stimulated with SR1, AhR expression in the nucleus decreased significantly, and in contrast, AhR expression in the cytoplasm increased (Figure 3B). This suggests that at lower concentrations, SR1 inhibits nuclear translocation of AhR in a concentration-dependent manner. Moreover, we were surprised to find that SR1 can significantly inhibit c-src phosphorylation in BMMs (Figures 3C and 3D). Previous studies have found that p-*c*-src can activate the NF-κB pathway and *p*-ERK MAPK pathway.[28–30] We also know about the MAPKs family and NF-κB signaling pathway from previous reports in the literature play an important role in the process of osteoclasts differentiation.[31] We hypothesize that SR1 blocks the activation of NF-κB and MAPK pathways by inhibiting c-src phosphorylation. To test our hypothesis, BMMs were treated with RANKL for 0, 15, 30, 45, and 60 min, with or without SR1. The results showed that the phosphorylation level of p-P65 had the most significant inhibitory effect by SR1 at the 15, 30 and 45 min, and the phosphorylation level of extracellular signal-regulated kinase (ERK) had the most significant inhibitory effect by SR1 at the 15 min (Figures 3E and 3F), while the phosphorylated protein expression levels of p-P38 and *p*-JNK did not change significantly (Figures S3A and S3B). Therefore, we found that the low concentration of SR1 inhibits the phosphorylation of c-src by inhibiting the nuclear translocation of AhR, and ultimately regulates the activation of the NF-κB and *p*-ERK/MAPK pathways.

SR1 did not influence osteogenic differentiation of OB cells after inhibiting AhR expression

SR1 has a significant inhibitory effect on osteoclasts differentiation. To study the effect of SR1 on osteogenic differentiation, osteoblast (OB cells) were treated with different concentrations of SR1 for 48 h and 96 h to determine the toxic effect of SR1 on OB cells. The results showed that SR1 had no effect on the proliferation activity of OB cells when the concentration of SR1 was less than 4 μM (Figure 4A). Primary osteoblasts were induced to differentiate by vitamin C and β-glycerosodium phosphate salts, and different concentrations of SR1 were added to stimulate for 14 days and 21 days. The alkaline phosphatase (ALP) staining results and the ARS staining results showed that the effects of different concentrations of drugs on osteogenic differentiation were similar compared with the control group (Figures 4B–4E), While the expression levels of bone-specific genes ALP, OPN, RUNX2, and OCN were not affected after 7 days of SR1 stimulation (Figure 4F). Therefore, SR1 does not influence osteogenic differentiation of primary osteoblasts within the safe toxicity range of OB cells.

SR1 inhibits OVX-induced bone loss *in vivo*

Previously, we studied the effect of SR1 on osteoclasts and osteoblast differentiation *in vitro*. Considering the complex physiological activities in animals, we selected 8-week-old female mice for this purpose and removed their bilateral ovaries to construct a mouse model of

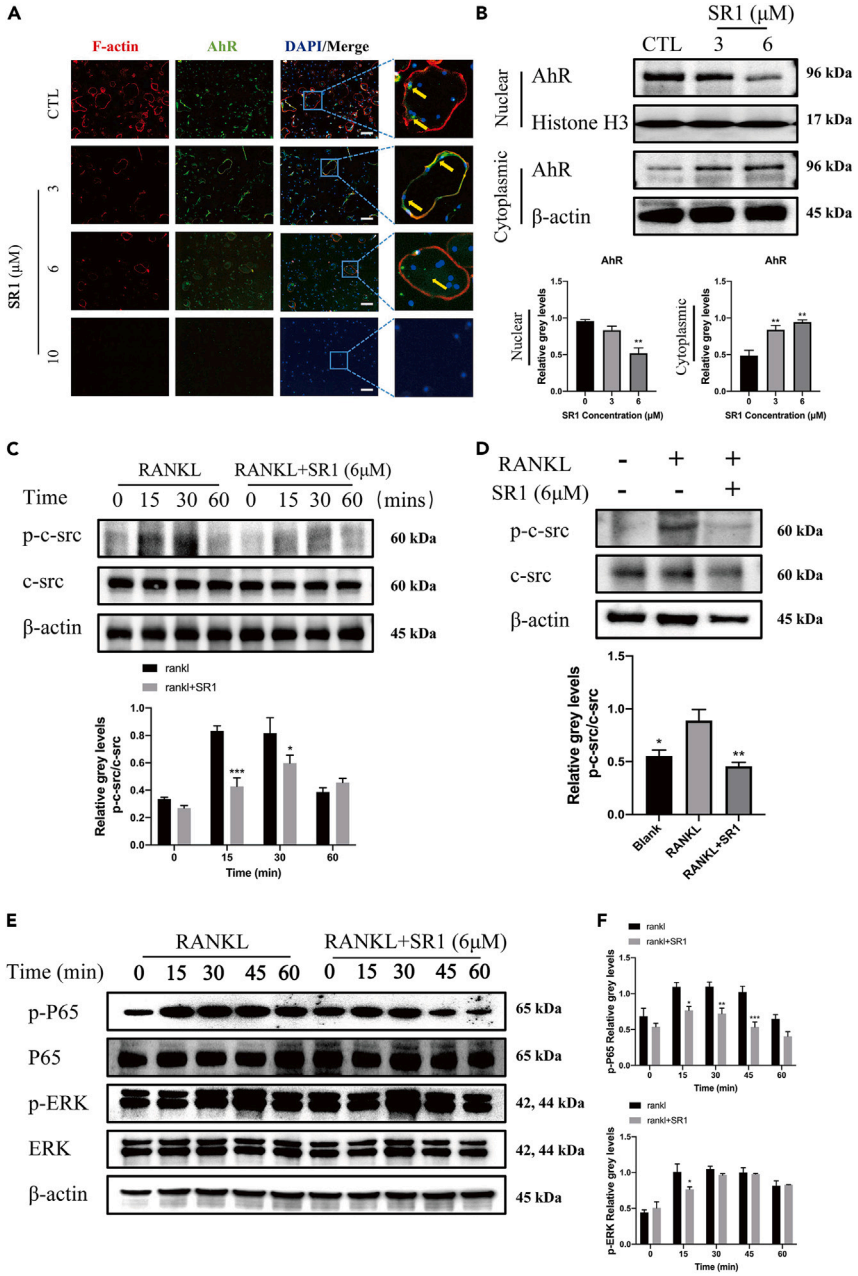

Figure 3. SR 1 attenuates the RANKL-induced osteoclastogenesis via inhibiting AhR-c-src-NF-κB/p-ERK MAPK-NFATc1 signaling pathway

(A) The BMMs were stimulated with the indicated concentrations of SR1. The detection of the AhR carried out immunofluorescence, Scale bar, 100 μm.

(B) BMMs were induced RANKL and stimulated with the indicated concentrations of SR1 for 4 days. The AhR protein levels in the cytoplasmic and nuclear were evaluated.

(C) BMMs were planted in a 6-well plate until the cells confluency reaches 90%, treated with serum-free medium starvation for 2 h, and then replaced with serum-containing medium and pretreated with or without 6 μM SR1 for 2 h. Finally, RANKL was stimulated the cells for 0, 15, 30, and 60 min. The cells were lysed with RIPA and the c-src and p-c-src protein levels were evaluated.

(D) BMMs were planted in a 6-well plate until the cells confluency reaches 90%, treated with serum-free medium starvation for 2 h, and then replaced with serum-containing medium and pretreated with or without 6 μM SR1 for 2 h. Finally, the cells were stimulated with or without RANKL for 15 min. The cells were lysed with RIPA and the c-src and p-c-src protein levels were evaluated.

(E) Treatment of BMMs was carried out with RANKL, with or without 6 μM SR1 for 0, 15, 30, 45, and 60 min. The p-P65, P65, *p*-ERK, and ERK protein levels were evaluated.

(F) Quantitative analysis results of p-P65, *p*-ERK relative to P65, ERK ratios are displayed. Data were presented as means ± SEM; $n = 3$; *$p < 0.05$, **$p < 0.01$, ***$p < 0.001$, ****$p < 0.0001$.

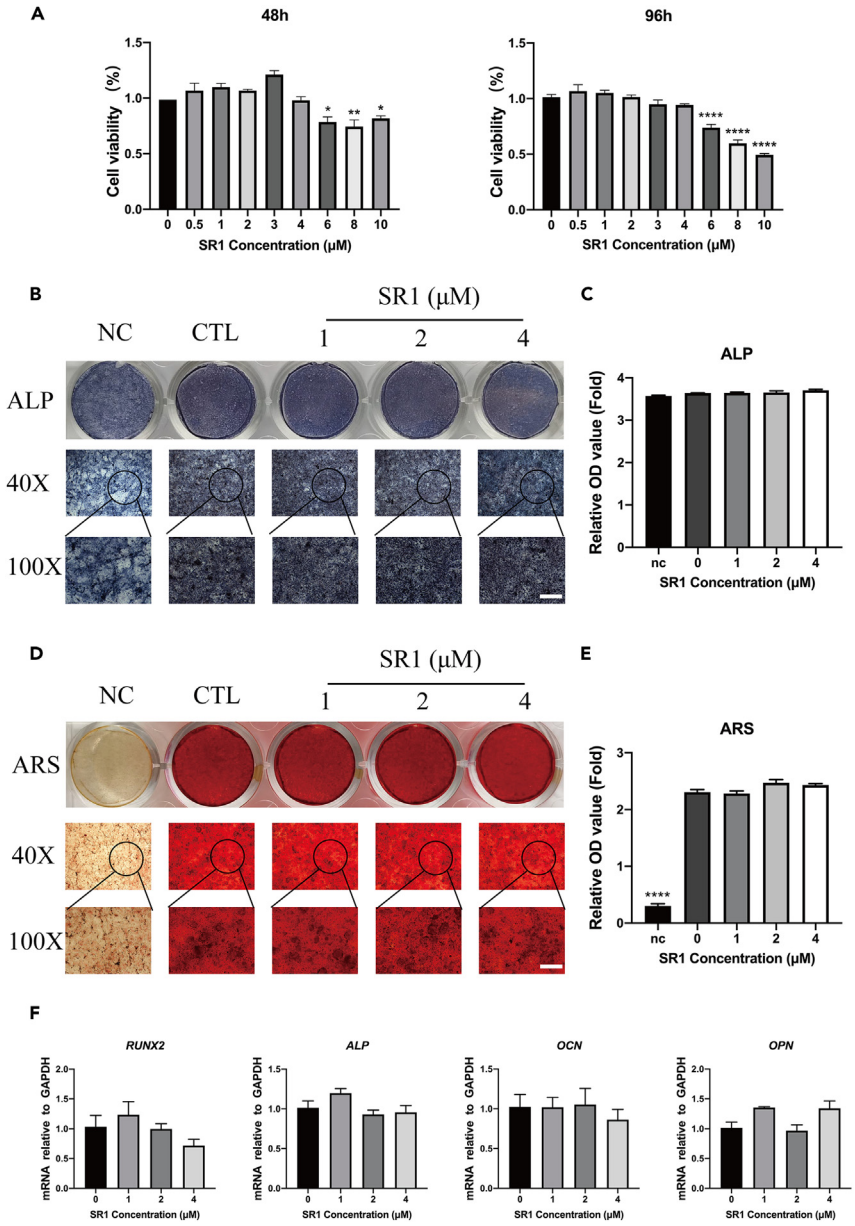

Figure 4. SR1 has no inhibitory effect on osteoblast differentiation

(A) Cell viability of primary osteoblasts with SR1 treated for 48 h and 96 h.

(B) After stimulating primary osteoblasts with osteogenesis induction solution (50 μg/mL vitamin C, 10 mM β-glycerol) and different concentrations of SR1 for 14 days. Representative image of ALP staining to show osteogenesis differentiation results, Scale bar, 200 μm.

(C) ALP activity was detected at different concentrations of SR1 after stimulating primary osteoblasts for 14 days.

(D) After stimulating primary osteoblasts with osteogenesis induction solution (50 μg/mL vitamin C, 10 mM β-glycerol) and different concentrations of SR1 for 21 days. Representative image of ARS staining to show osteogenesis differentiation results, Scale bar = 200 μm.

(E) ARS activity was detected at different concentrations of SR1 after stimulating primary osteoblasts for 21 days.

(F) Primary osteoblasts were stimulated with the indicated different concentrations of SR1 for 7 days, using qPCR to show the mRNA level of the osteoblast-specific genes, including ALP, Runx2, OPN, and OCN, normalized to GAPDH. The Data were presented as means ± SEM; $n = 3$; *$p < 0.05$, **$p < 0.01$, ****$p < 0.0001$.

osteoporosis (OVX group), studied the effect of SR1 in mice, and recorded the weight changes of mice at 7 weeks after administration. It was found that OVX mice gained weight significantly faster than sham group, and SR1 treatment had no effect on the weight of mice (Figure 5A). Protein and RNA were extracted from the isolated mouse forelimbs. Western Blot (WB) and qPCR analysis showed that the expression of AhR

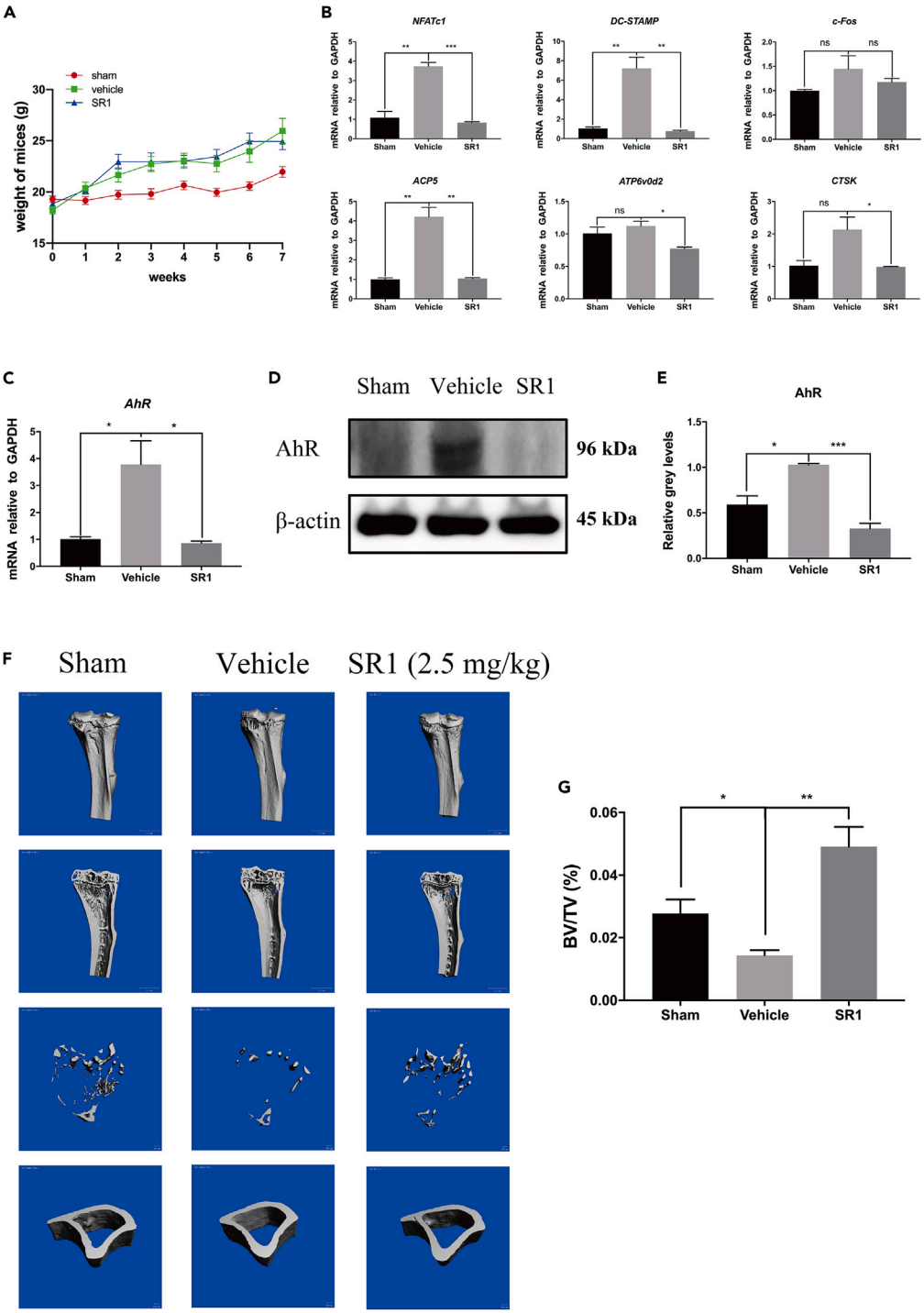

Figure 5. Evaluation and analysis of OVX-induced model via micro CT mainly

(A) Weight change diagram of C57BL/6J mice before and after OVX surgery.

(B and C) Tissue total RNA was extracted from Mice forelimb, and the mRNA expression levels of AhR, CTSK, NFATc1, DC-STAMP, ACP5, c-Fos, and ATP6v0d2 were displayed by qPCR, normalized to GAPDH.

(D and E) Mice forelimb bone tissue was isolated of from each experimental group. Adding tissue lysate to extract tissue protein, AhR specific primary antibody was used to show the results by western blot.

(F and G) The micro-CT was used to scan tibias of each mouse, and trabecular bone volume per total volume (BV/TV) was recorded for each specimen. And the relative data are compared. The Data were presented as means ± SEM; $n = 3$, $^{*}p < 0.05$, $^{**}p < 0.01$, $^{****}p < 0.0001$.

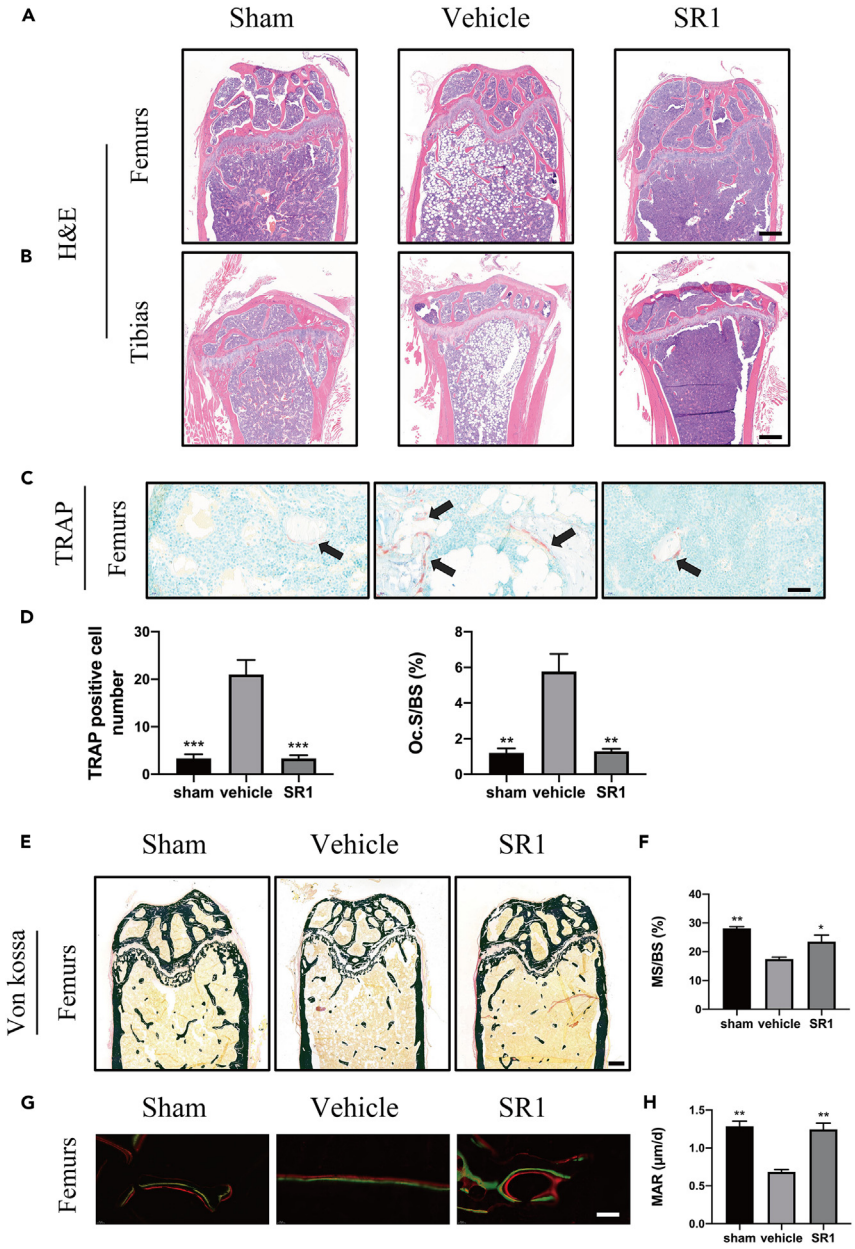

Figure 6. SR1 inhibits bone loss in OVX mice

(A and B) H&E staining results detect bone mass loss (Femur and tibia).

(C and D) TRAP staining was used for sections of femurs. The number of osteoclasts and the area of osteoclasts per field of each specimen were measured.

(E and F) The von Kossa staining was used for the sections of femurs and the mineralized surface area/bone surface area (MS/BS (%)) was measured.

(G and H) Calcein-alizarin red S labeling to detect the femur mineral apposition rate (MAR) in mice. Scale bar, 100 μm. Data were presented as means ± SEM; $n = 3$; *$p < 0.05$, **$p < 0.01$, ****$p < 0.0001$.

protein and gene in OVX group were significantly increased compared with those in sham group. The expression of AhR protein and gene were inhibited after SR1 treatment in OVX group (Figures 5C–5E). Meanwhile, we found that after SR1 treatment, compared with the vehicle group, the expressions of osteoclasts specific genes CTSK, DC-stamp, ACP5, NFATc1, and ATP6v0d2 were significantly downregulated (Figure 5B). At the same time, micro CT showed obvious bone loss in tibia of OVX-induced osteoporotic animals. And SR1 treatment group significantly saved bone loss in mice (Figures 5F and 5G). We found that histological analysis of the tibia and femur using H&E staining showed that SR1 reduced bone loss in mice (Figures 6A and 6B). Similarly, TRAP staining presented that more TRAP-positive mature osteoclasts in OVX mice, while there were fewer stained osteoclasts in SR1-treatment group (Figures 6C and 6D). To further study the effect of SR1 on osteoblast

formation, von Kossa staining and Calcein-alizarin red S labeling were occupied to examine femoral mineralization area and deposition rate, respectively. The von Kossa staining of femurs demonstrated that in the OVX group, the ratio of mineralized area (black part of the trabecular bone region) to bone area of distal femur decreased, while SR1 treatment can improve this ratio (Figures 6E and 6F). Calcein-alizarin red S labeling showed that the mineral apposition rate (MAR) of the femur was remarkably improved by SR1 when compared with the vehicle group (Figures 6G and 6H). And no toxic effects were identified in major organs (Figure S3C). Taken together, these results demonstrate that SR1 can inhibit osteoclasts activity and promote osteoblast activity *in vivo*, thereby reducing OVX-induced bone loss.

DISCUSSION

Human bone tissue is constantly remodeled throughout life, and the dynamic balance of osteoclasts and osteoblasts maintains the stability of bones. Excessive activation of osteoclasts will lead to the breakdown of this balance, which will lead to many bone diseases.[7] Aging and a drop in estrogen levels during the menopause are common causes of osteoporosis.[1] For this reason, in recent years, a variety of drugs and targets for the treatment of osteoporosis have emerged, such as estrogen replacement therapy and drugs like dihydric phosphate. These drugs have some side effects such as vaginal bleeding and deep vein thrombosis,[32] breast cancer,[33] osteonecrosis of the mandible[34] etc. Additional treatments are needed to alleviate these side effects, so the scope of use of these drugs is limited. Therefore, we are trying to find new therapeutic targets for osteoporosis and their corresponding drugs. Previous studies have known that the change of AhR expression is related to the occurrence of osteoclasts, but the specific relationship is still controversial in different studies, and the effect of the activation of AhR pathway on osteoporosis and osteoclasts is also different. And previous studies have not clearly explained how the AhR pathway affects osteoporosis.[23,27,35,36] In this study, we fully explored the important role of AhR in bone metabolism *in vitro* and *in vivo*. And we found SR1, a specific inhibitor of AhR can inhibit the phosphorylation of c-src by inhibiting the nuclear translocation of AhR, and ultimately regulates the activation of the NF-κB and *p*-ERK/MAPK pathways for the first time, while not inhibiting the occurrence of osteogenesis. At the same time, we successfully used SR1 to save bone loss in ovx mice *in vivo*.

In our experiments, SR1, previously a purine derivative, was first identified in an unbiased screening of a compound that promotes the expansion of $CD34^+$ hematopoietic progenitors. *In vitro* expansion of $CD34^+$ cells was promoted by inhibiting AhR expression,[18] and Phase I/II trials of expanded cord blood hematopoietic stem cells with SR1 support testing as standalone grafts.[37] Therefore, we tried to test the effect of SR1 on osteoclasts genesis and further study the relationship between SR1 and osteoporosis and its specific mechanism. It was found that during normal osteoclasts development, AhR would break away from the stable complex structure in the cytoplasm and enter the nucleus to play a role, which was also confirmed in the previous literature.[38] In our current study, we found that treating BMMs with 6 μM SR1 can inhibit cytoplasmic AhR from entering the nucleus. However, how this process occurs remains to be further investigated in the future.

In addition, when we used Norisoboldine to stimulate the differentiation of BMM cells into osteoclasts, we found that Norisoboldine significantly promoted the formation of osteoclasts in a concentration-dependent manner, which was quite contrary to the results of previous studies.[35] We suspect that this may be due to differences in the type of cells treated and the dosage of Norisoboldine. In addition, we also found that early suppression of AhR had the greatest effect on inhibiting osteoclasts formation, indicating that AhR was mainly involved in the early stage of osteoclasts differentiation. According to our study and previous literature reports,[25,26] we guessed that the early stage of osteoclast differentiation is the period most susceptible to external factors. The signal pathways of osteoclasts formation have formed a complex network with the diversities of explorations and researches. The NF-κB, MAPK protein family is two important signaling pathways for osteoclasts formation. The MAPK family, including ERKs, JNKs, and P38, is phosphorylated under RANKL stimulation and is involved in osteoclasts differentiation. In addition, blocking the NF-κB signaling pathway can inhibit osteoclastogenesis and promote osteogenesis.[39,40] The results of WB in the experiment proved that SR1 inhibits the phosphorylation of c-src by inhibiting the nuclear translocation of AhR, and ultimately regulates the activation of the NF-κB and *p*-ERK/MAPK pathways. Numerous studies have demonstrated that NFATc1 is a key transcription factor for osteoclasts differentiation and is capable of continuous self-amplification.[41,42] However, SR1 did not promote osteogenesis *in vitro*, which we speculated was due to the co-regulation of multiple factors. This needs to be further explored.[8]

In summary, we found that in the natural environment, there are ligands of AhR in environmental pollutants, which can activate AhR, and AhR in the activated state can promote the expression of osteoclast differentiation-associated genes and the formation of osteoclasts after entering the nucleus. Our study demonstrates for the first time that SR1 can inhibit c-src phosphorylation by inhibiting nuclear translocation of AhR. P-*c*-src is a protein kinase, and inhibition of p-*c*-src prevents the activation of NF-κB and pERK/MAPK pathways, ultimately inhibiting osteoclast formation and bone resorption (Figure 7). Therefore, SR1 can inhibit bone loss by inhibiting nuclear translocation of AhR, which has a therapeutic effect on osteoporosis and discovers a new therapeutic target for the study of bone metabolic diseases.

Limitations of the study

Our study also has some problems worth further research. AhR can regulate the direction of T cell differentiation, and the direction of T cell differentiation has two completely different directions.[43] This leads to changes in inflammatory factors in the organism. Activation of AhR also leads to the production of ROS,[38] ROS can activate the downstream MAPK signaling pathway and promote osteoclasts formation.[44] Therefore, the activation of AhR pathway leading to the increase of ROS and inflammatory factors may also have some influence on bone loss in mice.[45,46]

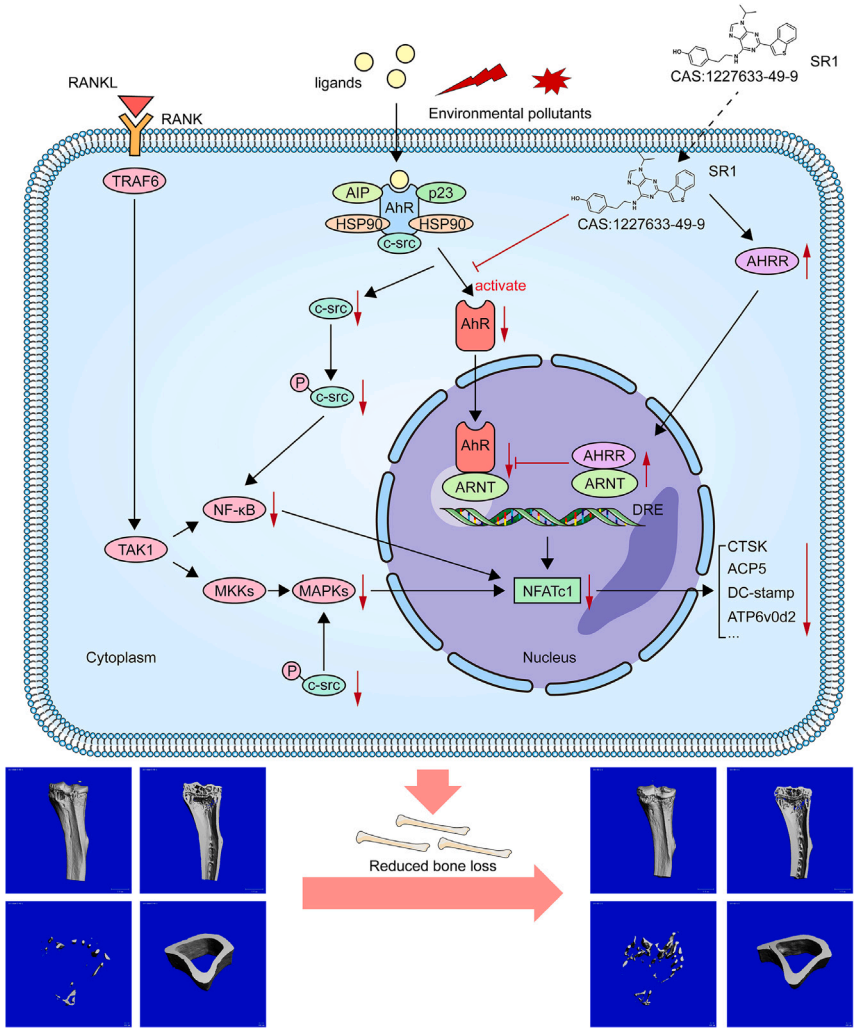

Figure 7. Mechanism diagram of SR1 alleviating bone loss

In the natural environment, air pollutants contain different AhR ligands. When these ligands enter the cell, they bind specifically to the stable inactive AhR complex in the cytoplasm. AhR is released from the stable complex structure, and the activated AhR is transferred to the nucleus to promote the expression of the downstream osteoclast differentiation-associated gene NFATc1. At the same time, c-src is also released from the stable complex structure, and c-src is phosphorylated to form p-c-src, which promotes the expression of NFATc1 by activating the NF-κB and MAPKs pathways. This promotes the formation of osteoclasts, which ultimately leads to bone loss. Low concentrations of SR1 can prevent the dissociation of c-src in the AhR complex, resulting in a decrease in free c-src and p-c-src. The decrease in p-c-src expression can inhibit the activation of the NF-κB and MAPKs pathways, while high concentrations of SR1 can directly inhibit the transcription of NFATc1 by suppressing the expression of AhR, and ultimately alleviate bone loss.

STAR★METHODS

Detailed methods are provided in the online version of this paper and include the following:

- KEY RESOURCES TABLE
- RESOURCE AVAILABILITY
  - Lead contact
  - Materials availability
  - Data and code availability
- EXPERIMENTAL MODEL AND STUDY PARTICIPANT DETAILS
  - Cell isolation and culture
  - Ovariectomized (OVX)-induced bone loss mouse model
- METHOD DETAILS
  - Flow cytometry

- Cell counting Kit-8 assay
- *In vitro* osteoclastogenesis assay and osteoclast count
- Osteoblast differentiation
- Cell transfection
- RNA extraction and quantitative real-time PCR (qPCR)
- Protein extraction and western blotting
- Fluorescent staining and actin ring formation of osteoclasts
- Micro-CT scanning
- Histological analysis (TRAP and H&E staining)
- Calcein-alizarin red S labeling and von Kossa staining

● QUANTIFICATION AND STATISTICAL ANALYSIS

SUPPLEMENTAL INFORMATION

Supplemental information can be found online at https://doi.org/10.1016/j.isci.2024.109682.

ACKNOWLEDGMENTS

This work was supported by Zhejiang Provincial Natural Science Foundation of China (LGF22H060003).

AUTHOR CONTRIBUTIONS

F.Z. and X.L. contributed to the study conception and design. Material preparation, experiments conduction and data collection were performed by S.Z., J.L., and T.Y. Statistical analysis was performed by Y.W. and Q.W. S.Z. wrote the first draft of the manuscript and X.L. revised the manuscript. All authors read and approved the final manuscript.

DECLARATION OF INTERESTS

The authors declare no competing interests.

Received: September 16, 2023
Revised: November 20, 2023
Accepted: April 3, 2024
Published: April 6, 2024

REFERENCES

1. Compston, J.E., McClung, M.R., and Leslie, W.D. (2019). Osteoporosis. Lancet *393*, 364–376. https://doi.org/10.1016/s0140-6736(18)32112-3.
2. Raggatt, L.J., and Partridge, N.C. (2010). Cellular and molecular mechanisms of bone remodeling. J. Biol. Chem. *285*, 25103–25108. https://doi.org/10.1074/jbc.R109.041087.
3. Lindsay, R. (1996). The menopause and osteoporosis. Obstet. Gynecol. *87*, 16S–19S. https://doi.org/10.1016/0029-7844(95)00430-0.
4. Soysa, N.S., Alles, N., Aoki, K., and Ohya, K. (2012). Osteoclast formation and differentiation: an overview. J. Med. Dent. Sci. *59*, 65–74.
5. Teitelbaum, S.L., and Ross, F.P. (2003). Genetic regulation of osteoclast development and function. Nat. Rev. Genet. *4*, 638–649. https://doi.org/10.1038/nrg1122.
6. Mundy, G.R. (2007). Osteoporosis and Inflammation. Nutr. Rev. *65*, 147–151. https://doi.org/10.1301/nr.2007.dec.S147-S151.
7. Boyce, B.F. (2013). Advances in osteoclast biology reveal potential new drug targets and new roles for osteoclasts. J. Bone Miner. Res. *28*, 711–722. https://doi.org/10.1002/jbmr.1885.
8. Xu, H., Wang, W., Liu, X., Huang, W., Zhu, C., Xu, Y., Yang, H., Bai, J., and Geng, D. (2023). Targeting strategies for bone diseases: signaling pathways and clinical studies. Signal Transduct. Target. Ther. *8*, 202. https://doi.org/10.1038/s41392-023-01467-8.
9. Huang, F., Wong, P., Li, J., Lv, Z., Xu, L., Zhu, G., He, M., and Luo, Y. (2022). Osteoimmunology: The correlation between osteoclasts and the Th17/Treg balance in osteoporosis. J. Cell Mol. Med. *26*, 3591–3597. https://doi.org/10.1111/jcmm.17399.
10. Asagiri, M., Sato, K., Usami, T., Ochi, S., Nishina, H., Yoshida, H., Morita, I., Wagner, E.F., Mak, T.W., Serfling, E., and Takayanagi, H. (2005). Autoamplification of NFATc1 expression determines its essential role in bone homeostasis. J. Exp. Med. *202*, 1261–1269. https://doi.org/10.1084/jem.20051150.
11. Neavin, D.R., Liu, D., Ray, B., and Weinshilboum, R.M. (2018). The Role of the Aryl Hydrocarbon Receptor (AHR) in Immune and Inflammatory Diseases. Int. J. Mol. Sci. *19*, 3851. https://doi.org/10.3390/ijms19123851.
12. Kewley, R.J., Whitelaw, M.L., and Chapman-Smith, A. (2004). The mammalian basic helix–loop–helix/PAS family of transcriptional regulators. Int. J. Biochem. Cell Biol. *36*, 189–204. https://doi.org/10.1016/s1357-2725(03)00211-5.
13. Tanaka, S., Amling, M., Neff, L., Peyman, A., Uhlmann, E., Levy, J.B., and Baron, R. (1996). c-Cbl is downstream of c-Src in a signalling pathway necessary for bone resorption. Nature *383*, 528–531. https://doi.org/10.1038/383528a0.
14. Rothhammer, V., and Quintana, F.J. (2019). The aryl hydrocarbon receptor: an environmental sensor integrating immune responses in health and disease. Nat. Rev. Immunol. *19*, 184–197. https://doi.org/10.1038/s41577-019-0125-8.
15. Jackson, C.S., Durandt, C., Janse van Rensburg, I., Praloran, V., Brunet de la Grange, P., and Pepper, M.S. (2017). Targeting the aryl hydrocarbon receptor nuclear translocator complex with DMOG and Stemregenin 1 improves primitive hematopoietic stem cell expansion. Stem Cell Res. *21*, 124–131. https://doi.org/10.1016/j.scr.2017.04.007.
16. Zhu, X., Sun, Q., Tan, W.S., and Cai, H. (2021). Reducing TGF-beta1 cooperated with StemRegenin 1 promoted the expansion ex vivo of cord blood CD34(+) cells by inhibiting AhR signalling. Cell Prolif. *54*, e12999. https://doi.org/10.1111/cpr.12999.
17. Singh, J., Chen, E.L.Y., Xing, Y., Stefanski, H.E., Blazar, B.R., and Zúñiga-Pflücker, J.C. (2019). Generation and function of progenitor T cells from StemRegenin-1-expanded CD34+ human hematopoietic progenitor cells. Blood Adv. *3*, 2934–2948. https://doi.org/10.1182/bloodadvances.2018026575.

18. Boitano, A.E., Wang, J., Romeo, R., Bouchez, L.C., Parker, A.E., Sutton, S.E., Walker, J.R., Flaveny, C.A., Perdew, G.H., Denison, M.S., et al. (2010). Aryl hydrocarbon receptor antagonists promote the expansion of human hematopoietic stem cells. Science *329*, 1345–1348. https://doi.org/10.1126/science.1191536.
19. Thordardottir, S., Hangalapura, B.N., Hutten, T., Cossu, M., Spanholtz, J., Schaap, N., Radstake, T.R.D.J., van der Voort, R., and Dolstra, H. (2014). The aryl hydrocarbon receptor antagonist StemRegenin 1 promotes human plasmacytoid and myeloid dendritic cell development from CD34+ hematopoietic progenitor cells. Stem Cells Dev. *23*, 955–967. https://doi.org/10.1089/scd.2013.0521.
20. Chen, Y., Dong, Y., Lu, X., Li, W., Zhang, Y., Mao, B., Pan, X., Li, X., Zhou, Y., An, Q., et al. (2022). Inhibition of aryl hydrocarbon receptor signaling promotes the terminal differentiation of human erythroblasts. J. Mol. Cell Biol. *14*, mjac001. https://doi.org/10.1093/jmcb/mjac001.
21. Lim, H.J., Jang, W.B., Rethineswaran, V.K., Choi, J., Lee, E.J., Park, S., Jeong, Y., Ha, J.S., Yun, J., Choi, Y.J., et al. (2023). StemRegenin-1 Attenuates Endothelial Progenitor Cell Senescence by Regulating the AhR Pathway-Mediated CYP1A1 and ROS Generation. Cells *12*, 2005. https://doi.org/10.3390/cells12152005.
22. Izawa, T., Arakaki, R., Mori, H., Tsunematsu, T., Kudo, Y., Tanaka, E., and Ishimaru, N. (2016). The Nuclear Receptor AhR Controls Bone Homeostasis by Regulating Osteoclast Differentiation via the RANK/c-Fos Signaling Axis. J. Immunol. *197*, 4639–4650. https://doi.org/10.4049/jimmunol.1600822.
23. Kim, S.Y., Oh, Y., Jo, S., Ji, J.D., and Kim, T.H. (2021). Inhibition of Human Osteoclast Differentiation by Kynurenine through the Aryl-Hydrocarbon Receptor Pathway. Cells *10*, 3498. https://doi.org/10.3390/cells10123498.
24. Liu, W.C., Shyu, J.F., Lim, P.S., Fang, T.C., Lu, C.L., Zheng, C.M., Hou, Y.C., Wu, C.C., Lin, Y.F., and Lu, K.C. (2020). Concentration and Duration of Indoxyl Sulfate Exposure Affects Osteoclastogenesis by Regulating NFATc1 via Aryl Hydrocarbon Receptor. Int. J. Mol. Sci. *21*, 3486. https://doi.org/10.3390/ijms21103486.
25. Li, J., Li, X., Zhou, S., Wang, Y., Lu, Y., Wang, Q., and Zhao, F. (2022). Tetrandrine inhibits RANKL-induced osteoclastogenesis by promoting the degradation of TRAIL. Mol. Med. *28*, 141. https://doi.org/10.1186/s10020-022-00568-4.
26. Li, X., Wang, Y., Li, L., Zhou, S., and Zhao, F. (2021). Sclareol inhibits RANKL-induced osteoclastogenesis and promotes osteoblastogenesis through promoting CCN1 expression via repressing the MAPK pathway. Cell Biol. Toxicol. *37*, 849–871. https://doi.org/10.1007/s10565-020-09578-6.
27. Jia, Y., Tao, Y., Lv, C., Xia, Y., Wei, Z., and Dai, Y. (2019). Tetrandrine enhances the ubiquitination and degradation of Syk through an AhR-c-src-c-Cbl pathway and consequently inhibits osteoclastogenesis and bone destruction in arthritis. Cell Death Dis. *10*, 38. https://doi.org/10.1038/s41419-018-1286-2.
28. Ren, Q., Guo, F., Tao, S., Huang, R., Ma, L., and Fu, P. (2020). Flavonoid fisetin alleviates kidney inflammation and apoptosis via inhibiting Src-mediated NF-kappaB p65 and MAPK signaling pathways in septic AKI mice. Biomed. Pharmacother. *122*, 109772. https://doi.org/10.1016/j.biopha.2019.109772.
29. Singer, C.A., Lontay, B., Unruh, H., Halayko, A.J., and Gerthoffer, W.T. (2011). Src mediates cytokine-stimulated gene expression in airway myocytes through ERK MAPK. Cell Commun. Signal. *9*, 14. https://doi.org/10.1186/1478-811X-9-14.
30. Li, Y., Xi, Z., Chen, X., Cai, S., Liang, C., Wang, Z., Li, Y., Tan, H., Lao, Y., and Xu, H. (2018). Natural compound Oblongifolin C confers gemcitabine resistance in pancreatic cancer by downregulating Src/MAPK/ERK pathways. Cell Death Dis. *9*, 538. https://doi.org/10.1038/s41419-018-0574-1.
31. Qiu, J., Jiang, T., Yang, G., Gong, Y., Zhang, W., Zheng, X., Hong, Z., and Chen, H. (2022). Neratinib exerts dual effects on cartilage degradation and osteoclast production in Osteoarthritis by inhibiting the activation of the MAPK/NF-kappaB signaling pathways. Biochem. Pharmacol. *205*, 115155. https://doi.org/10.1016/j.bcp.2022.115155.
32. Grodstein, F., Stampfer, M.J., Goldhaber, S.Z., Manson, J.E., Colditz, G.A., Speizer, F.E., Willett, W.C., and Hennekens, C.H. (1996). Prospective study of exogenous hormones and risk of pulmonary embolism in women. Lancet *348*, 983–987. https://doi.org/10.1016/S0140-6736(96)07308-4.
33. Franceschini, G., Lello, S., and Masetti, R. (2020). Hormone replacement therapy: revisiting the risk of breast cancer. Eur. J. Cancer Prev. *29*, 303–305. https://doi.org/10.1097/CEJ.0000000000000548.
34. Bamias, A., Kastritis, E., Bamia, C., Moulopoulos, L.A., Melakopoulos, I., Bozas, G., Koutsoukou, V., Gika, D., Anagnostopoulos, A., Papadimitriou, C., et al. (2005). Osteonecrosis of the Jaw in Cancer After Treatment With Bisphosphonates: Incidence and Risk Factors. J. Clin. Oncol. *23*, 8580–8587. https://doi.org/10.1200/jco.2005.02.8670.
35. Wei, Z.F., Lv, Q., Xia, Y., Yue, M.F., Shi, C., Xia, Y.F., Chou, G.X., Wang, Z.T., and Dai, Y. (2015). Norisoboldine, an Anti-Arthritis Alkaloid Isolated from Radix Linderae, Attenuates Osteoclast Differentiation and Inflammatory Bone Erosion in an Aryl Hydrocarbon Receptor-Dependent Manner. Int. J. Biol. Sci. *11*, 1113–1126. https://doi.org/10.7150/ijbs.12152.
36. Eisa, N.H., Reddy, S.V., Elmansi, A.M., Kondrikova, G., Kondrikov, D., Shi, X.M., Novince, C.M., Hamrick, M.W., McGee-Lawrence, M.E., Isales, C.M., et al. (2020). Kynurenine Promotes RANKL-Induced Osteoclastogenesis In Vitro by Activating the Aryl Hydrocarbon Receptor Pathway. Int. J. Mol. Sci. *21*, 7931. https://doi.org/10.3390/ijms21217931.
37. Wagner, J.E., Jr., Brunstein, C.G., Boitano, A.E., DeFor, T.E., McKenna, D., Sumstad, D., Blazar, B.R., Tolar, J., Le, C., Jones, J., et al. (2016). Phase I/II Trial of StemRegenin-1 Expanded Umbilical Cord Blood Hematopoietic Stem Cells Supports Testing as a Stand-Alone Graft. Cell Stem Cell *18*, 144–155. https://doi.org/10.1016/j.stem.2015.10.004.
38. Vogel, C.F.A., Van Winkle, L.S., Esser, C., and Haarmann-Stemmann, T. (2020). The aryl hydrocarbon receptor as a target of environmental stressors - Implications for pollution mediated stress and inflammatory responses. Redox Biol. *34*, 101530. https://doi.org/10.1016/j.redox.2020.101530.
39. Boyle, W.J., Simonet, W.S., and Lacey, D.L. (2003). Osteoclast differentiation and activation. Nature *423*, 337–342. https://doi.org/10.1038/nature01658.
40. Bai, J., Wang, H., Chen, H., Ge, G., Wang, M., Gao, A., Tong, L., Xu, Y., Yang, H., Pan, G., et al. (2020). Biomimetic osteogenic peptide with mussel adhesion and osteoimmunomodulatory functions to ameliorate interfacial osseointegration under chronic inflammation. Biomaterials *255*, 120197. https://doi.org/10.1016/j.biomaterials.2020.120197.
41. Takayanagi, H., Kim, S., Koga, T., Nishina, H., Isshiki, M., Yoshida, H., Saiura, A., Isobe, M., Yokochi, T., Inoue, J.i., et al. (2002). Induction and activation of the transcription factor NFATc1 (NFAT2) integrate RANKL signaling in terminal differentiation of osteoclasts. Dev. Cell *3*, 889–901. https://doi.org/10.1016/s1534-5807(02)00369-6.
42. Aliprantis, A.O., Ueki, Y., Sulyanto, R., Park, A., Sigrist, K.S., Sharma, S.M., Ostrowski, M.C., Olsen, B.R., and Glimcher, L.H. (2008). NFATc1 in mice represses osteoprotegerin during osteoclastogenesis and dissociates systemic osteopenia from inflammation in cherubism. J. Clin. Invest. *118*, 3775–3789. https://doi.org/10.1172/JCI35711.
43. Xie, J., Wang, Z., and Wang, W. (2020). Semaphorin 4D Induces an Imbalance of Th17/Treg Cells by Activating the Aryl Hydrocarbon Receptor in Ankylosing Spondylitis. Front. Immunol. *11*, 2151. https://doi.org/10.3389/fimmu.2020.02151.
44. Zhu, J., Yu, W., Liu, B., Wang, Y., Shao, J., Wang, J., Xia, K., Liang, C., Fang, W., Zhou, C., and Tao, H. (2017). Escin induces caspase-dependent apoptosis and autophagy through the ROS/p38 MAPK signalling pathway in human osteosarcoma cells in vitro and in vivo. Cell Death Dis. *8*, e3113. https://doi.org/10.1038/cddis.2017.488.
45. Arai, M., Shibata, Y., Pugdee, K., Abiko, Y., and Ogata, Y. (2007). Effects of reactive oxygen species (ROS) on antioxidant system and osteoblastic differentiation in MC3T3-E1 cells. IUBMB Life *59*, 27–33. https://doi.org/10.1080/15216540601156188.
46. Wang, Y., Li, X., Zhou, S., Li, J., Zhu, Y., Wang, Q., and Zhao, F. (2022). MCU Inhibitor Ruthenium Red Alleviates the Osteoclastogenesis and Ovariectomized Osteoporosis via Suppressing RANKL-Induced ROS Production and NFATc1 Activation through P38 MAPK Signaling Pathway. Oxid. Med. Cell. Longev. *2022*, 7727006. https://doi.org/10.1155/2022/7727006.
47. Zhang, X., Hou, L., Li, F., Zhang, W., Wu, C., Xiang, L., Li, J., Zhou, L., Wang, X., Xiang, Y., et al. (2022). Piezo1-mediated mechanosensation in bone marrow macrophages promotes vascular niche regeneration after irradiation injury. Theranostics *12*, 1621–1638. https://doi.org/10.7150/thno.64963.
48. Boerckel, J.D., Mason, D.E., McDermott, A.M., and Alsberg, E. (2014). Microcomputed tomography: approaches and applications in bioengineering. Stem Cell Res. Ther. *5*, 144. https://doi.org/10.1186/scrt534.

STAR★METHODS

KEY RESOURCES TABLE

REAGENT or RESOURCE	SOURCE	IDENTIFIER
Antibodies		
anti-GAPDH antibody	Cell Signaling Technology	Cat# 51332
anti-β-actin antibody	Cell Signaling Technology	Cat# 3700
anti-Histone H3 antibody	Cell Signaling Technology	Cat# 9715
anti-AhR antibody	Proteintech	Cat# 67785-1-Ig
anti-NFATc1 antibody	Proteintech	Cat# 66963-1-Ig
anti-CTSK antibody	Cell Signaling Technology	Cat# 57056
anti-ACP5 antibody	Proteintech	Cat# 11594-1-AP
anti-P65 antibody	Cell Signaling Technology	Cat# 4764
anti-p-P65 antibody	Cell Signaling Technology	Cat# 3033
anti-ERK antibody	Cell Signaling Technology	Cat# 4695
anti-*p*-ERK antibody	Cell Signaling Technology	Cat# 4370
anti-JNK antibody	Cell Signaling Technology	Cat# 9252
anti-*p*-JNK antibody	Cell Signaling Technology	Cat# 4668
anti-P38 antibody	Cell Signaling Technology	Cat# 9212
anti-p-P38 antibody	Cell Signaling Technology	Cat# 4511
anti-c-src antibody	Proteintech	Cat# 60315-1-Ig
anti-p-c-src antibody	Cell Signaling Technology	Cat# 2101
anti-AHRR antibody	Proteintech	Cat# 13241-1-AP
anti-c-Fos antibody	Cell Signaling Technology	Cat# 2250
Chemicals, peptides, and recombinant proteins		
PBS	Beyotime Biotechnology	Cat# P0010S
2×SYBR Green qPCR master mix	EZBioscience	Cat# A0001-R2
StemRegenin 1	Selleck	Cat# S2858
FBS	Thermo Fisher Scientific	Cat# 10099141
1% penicillin-streptomycin	Biological Industries	Cat# 03-031-1B
α-MEM	Thermo Fisher Scientific	Cat# 12561056
ECL Luminous Liquid	FD Biotech	Cat# FD8000
RIPA	Sigma-Aldrich	Cat# V900854
RANKL	R&D	Cat# 462-TEC
M-CSF	R&D	Cat# 416-ML
0.25% Trypsin	Beyotime Biotechnology	Cat# P0013B
Alizarin red S	Sigma-Aldrich	Cat# a5533-25g
EDTA	solarbio	Cat# E1171
Norisoboldine	Selleck	Cat# S9092
DMEM	Thermo Fisher Scientific	Cat# 11995065
DAPI	Beyotime Biotechnology	Cat# C1002
calcein	Sigma-Aldrich	Cat# C0875-5g
Critical commercial assays		
TRAP dyeing kit	Sigma-Aldrich	Cat# 387A-1KT
CCK-8 assay solution	solarbio	Cat# CA1210

(*Continued on next page*)

Continued

REAGENT or RESOURCE	SOURCE	IDENTIFIER
SDS-PAGE gel preparation kit	Beyotime Biotechnology	Cat# P0012A
RNAiso Plus Kit	Takara Bio	Cat# 9108
HiFiScipt cDNA Synthesis kit	CWBIO	Cat# CW0741M
bicinchoninic acid protein (BCA) assay kit	Millipore	Cat# BCA1
Experimental models: Organisms/strains		
Mouse: C57BL/6 mice	Animal Experiment Center, the First Affiliated Hospital of Zhejiang University School of Medicine	N/A
Oligonucleotides		
See Table S1	Tsingke Biotechnology	N/A
Software and algorithms		
GraphPad Prism version 9.0	GraphPad Software	N/A
FlowJo version 10.0	FlowJo Software	N/A
ImageJ software	NIH	N/A

RESOURCE AVAILABILITY

Lead contact

Further information and requests for resources and reagents should be directed to and will be fulfifilled by the lead contact, Dr. Fengchao Zhao (zhaofengchao@zju.edu.cn).

Materials availability

This study did not generate new unique reagents.

Data and code availability

- This paper does not report original code.
- Data reported in this paper will be shared by the lead contact upon request.
- Any additional information required to reanalyze the data reported in this paper is available from the lead contact upon request.

EXPERIMENTAL MODEL AND STUDY PARTICIPANT DETAILS

Cell isolation and culture

Eight-week-old C57BL/6 male mice was prepared for the extraction of bone marrow macrophages (BMMs). The mice were sacrificed by cervical dislocation, soaked in 75% alcohol for 10 min, then the lower limbs were separated with sterile scissors, the muscle tissue on the lower extremity surface was removed, and the femur and tibia were separated. The bone marrow was rinsed into a 10 cm Petri dish using a 1 mL syringe. The BMMs cells will be extracted to cultivated in an α-MEM medium (Gibco-BRL, Gaithersburg, MD, USA), FBS (10%) (Gibco-BRL, Gaithersburg, MD, USA), 1% penicillin/streptomycin (1%, Gibco-BRL, Gaithersburg, MD, USA), and 25 ng/mL M-CSF (R&D, Minneapolis, MN, USA) in 37°C and 5% CO_2 incubator. After 48 h, the medium was changed to remove the unattached cells and attached cells were used for subsequent experiments.

The mouse osteoblast cells were extracted from the skull of 8-day-old lactating mice. The lactating mice were first killed, soaked in 75% alcohol for 10 min and sterilized. The skulls of lactating mice were separated with sterile scissors, then the excess intracranial tissue was cut off and the skull was separated. Then the medium was changed into type 1 collagenase and digested in the incubator (37°C, 5% CO_2) for 12 h. Finally, the medium was replaced by DMEM supplemented with 10% FBS and 1% penicillin/streptomycin. After 48 h, the medium was changed to remove the unattached cells and attached cells were used for subsequent experiments.

Ovariectomized (OVX)-induced bone loss mouse model

8-week-old C57BL/6 female mice (n = 15) weighing 20 to 25 g were anesthetized with 3 mg/mL pentobarbital for bilateral ovariectomy (OVX). The mice were randomly divided into three groups (each; n = 5). The sham and vehicle group were injected with corn oil (MedChemExpress, NJ, USA) containing 10% DMSO (MedChemExpress), and the SR1 group was injected with SR1 (2.5 mg/kg) every 3 days for 42 days. Next, the isolated femur and tibia were fixed in 4% paraformaldehyde for 48 h and the micro-CT and histological experiments were carried out. The study protocol was approved by the Research Ethics Committee of the First Affiliated Hospital of Zhejiang University. All efforts were made to minimize the number and suffering of animals.

METHOD DETAILS

Flow cytometry

Bone marrow macrophages (BMMs) were extracted and cultured with 25 ng/mL M-CSF. After 96 h, BMMs were stained for 30 min at 4°C in the dark using the following antibodies: APC-Cy7 CD11b (101226), APC F4/80 (123116), all purchased from BioLegend (USA). 7-AAD (559925, B.D., USA) staining was used to identify living cells. Flow cytometry was performed on the Gallios Flow Cytometer (Beckman, USA). FlowJo Software Version 10 (FlowJo LLC, USA) was used for subsequent analyses.[47]

Cell counting Kit-8 assay

The cytotoxicity of SR1 to BMMs and OBs was determined by CCK-8 method. Simply put, 6×10^3 cells were added to each of the 96-well plates, With different concentrations of SR1 (Selleck, Houston, Texas, United States) of different concentrations for 48 and 96 h. Then, 10 μl CCK8 reagent (Solarbio, Beijing, China) was added to each well and cultured for 1 h. The absorbance value at 450 nm was detected by microplate reader (Bio-Tek Instruments, Winooski, VT, USA).

In vitro osteoclastogenesis assay and osteoclast count

In 96 well plates, 6×10^3 BMMs were added to each well and cultured for 12 h to adhere to the wall. BMMs were then incubated with 25 ng/mL M-CSF and 50 ng/mL RANKL (R&D, Minneapolis, MN, USA), and different concentrations of SR1 (0, 3, 6, 8, 10 μM) were added. The medium was changed every two days for 7 days, washed twice with PBS, fixed with 4% paraformaldehyde at room temperature for 15 min, washed twice with PBS, and finally stained with tartrate-resistant acid phosphatase (TRAP) (Sigma-Aldrich, St. Louis, MO, USA) at room temperature for 30 min. Osteoclasts were observed under a fluorescence microscope (NIKON TE2000, Nikon Corporation, Minato, Tokyo, Japan). The cell body of osteoclasts is large, and osteoclasts are multinucleated cells. We first photographed each group of osteoclasts under a fluorescence microscope, and then counted the number of osteoclasts with more than 3 nuclei by ImageJ software (NIH, Bethesda, MD, USA).

Osteoblast differentiation

Osteogenesis induction of OB cells was performed in DMEM medium containing 50 μg/mL ascorbic acid and 10 μM β-glycerophosphatester (Sigma-Aldrich, St. Louis, MO, USA). After 7 days of osteogenic induction, the expression levels of bone-specific genes were detected. After 14 days of osteogenic induction, alkaline phosphatase (ALP) staining was performed with a BCIP/NBT kit (CWBIO, Beijing, China), and ALP activity was quantified with an alkaline phosphatase assay kit (Beyotime, Nanjing, China). Alizarin red S (ARS) staining was performed with 1% alizarin red staining solution (Sigma-Aldrich, Shanghai, China) 21 days after osteogenesis induction to observe the mineralization deposition in the extracellular matrix. To quantify the mineralization, the absorbance at 405 nm was measured with a microplate reader (Bio-Tek Instruments) by elution staining with 10% glacial acetic acid.

Cell transfection

The BMMs were laid into 6-well plates, 12-well plates or 96-well plates, and the medium was changed once every two days. When the cell density reached 50–60%, they were stimulated with RANKL for 4 h, and then transfected with AhR siRNA (50 nM) or negative controls (control siRNA) for another 6 h, which were purchased from Tsingke Biotechnology Co (Beijing, China). Transfections were performed using TSnanofect transfection reagent (Tsingke Biotechnology Co, Beijing, China) according to the manufacturer's instructions. After that, the previous medium was replaced with the medium containing 25 ng/mL M-CSF and 50 ng/mL RANKL and continued for the specified time (The protein and RNA extraction experiments were cultured for 48 h, and the TRAP staining experiments were cultured for 5 days). AhR siRNA: sense (5′-3′) GAGGUUAAAGUAUCUUCAUTT, antisense (5′-3′) AUGAAGAUACUUUAACCUCTT.

RNA extraction and quantitative real-time PCR (qPCR)

The cultured cells were lysed with RNAiso Plus Kit (Takara Bio, Otsu, Japan) to extract total RNA, according to the manufacturer's protocol. Total RNA was reverse transcribed into cDNA using the HiFiScipt cDNA Synthesis kit (CWBIO). cDNA was amplified via quantitative real-time PCR. qPCR was performed using 2× SYBR qPCR Master Mix (EZBioscience, USA) with ABI Prism 7500 fast system (Applied Biosystems, Foster City, CA, USA). The conditions for PCR cycling were as follows: 95°C for 5 min, then the next step consists of 40 cycles at 95°C for 10 s and 60°C for 30 s, and a final step at 4°C for 10 min the expression level of each gene was calculated by the method of $2^{-\Delta\Delta Ct}$. The primer sequences were listed in Table 1.

Protein extraction and western blotting

Total protein was extracted from BMMs and OB cells and bones of mice used in the OVX experiment using radio immune precipitation assay lysis buffer (RIPA) (Sigma-Aldrich) and the protein concentration was measured using a bicinchoninic acid protein (BCA) assay kit (Millipore, Bedford, MA, USA). Equivalent amounts of protein via 10% SDS-PAGE and transferred to PVDF membranes (EMD Millipore). The membranes were blocked with 5% skim milk in Tris-buffered saline with Tween 20 at room temperature for 1 h. Following the overnight incubation of primary antibodies at 4°C, the membranes were nurtured with corresponding HRP-conjugated secondary antibodies (Proteintech Group, Chicago, IL, USA). The bands were visualized employing ECL Luminous Liquid (FDbio, Hangzhou, China). The gray level of proteins was

calculated by ImageJ software (NIH, Bethesda, MD, USA). The gray level of the target protein is compared with the gray level of the internal reference protein to obtain a value, and then the comparison value is compared with the comparison value of the CTL group, the result is the relative gray level. Anti-AhR (Cat No: 67785-1-Ig), AHRR (Cat No: 13241-1-AP), ACP5 (Cat No: 11594-1-AP), NFATc1 (Cat No: 66963-1-Ig), c-src (Cat No: 60315-1-Ig) were procured from Proteintech (Wuhan, China). Anti-GAPDH (Cat No: 51332), β-actin (Cat No: 3700), Histone H3 (Cat No: 9715), CTSK (Cat No: 57056), c-Fos (Cat No: 2250), p-P65 (Cat No: 3033), P65 (Cat No: 4764), p-P38 (Cat No: 4511), P38 (Cat No: 9212), *p*-JNK (Cat No: 4668), JNK (Cat No: 9252), *p*-ERK (Cat No: 4370), ERK (Cat No: 4695), p-*c*-src (Cat No: 2101) were all purchased from Cell Signaling Technology (Danvers, MA, USA).

Fluorescent staining and actin ring formation of osteoclasts

The BMMs were cultivated in the presence of SR1, using a 96-well plate. The cells washed with PBS three times, fixed in 4% paraformaldehyde for 15 min at room temperature. Triton X-100 (0.1%, v/v) was carried out for 20 min to permeabilize the cells. After blocking with goat serum, anti-AhR, NFATc1, CTSK antibody were added to cells overnight at 4°C followed by a goat anti-mouse Alexa Fluor-488-conjugated secondary antibody (Abcam). To visualize F-actin ring formation, rhodamine phalloidin was used for F-actin staining at room temperature away from light for an hour. After washed with PBS for three times, cells were then stained with DAPI (Beyotime Institute of Biotechnology, Shanghai, China) for 15 min at room temperature and observed under a fluorescence microscope (NIKON TE2000, Nikon Corporation, Minato, Tokyo, Japan).

Micro-CT scanning

Micro-CT scanner (1072 μCT System; Sky Scan, Bruker micro CT, Kontich, Belgium) was used to examine the fixed tibia according to a previously reported procedure.[48] The parameters are set as follows: The X-ray energy was 70 kV and 300 μA, the aluminum filter was 0.5 mm, the rotation step was 0.4°C and the isometric resolution was 9 μm. For reconstruction, the NRecon program (Bruker micro CT, kontich, Belgium) was put into use. For rebuilding, the settings are as follows: 1. Smoothing; 2. Ring artifact correction; 3. correction of beam hardening, 40%. Utilizing the software CTAn (Bruker micro CT, Kontich, Belgium), each sample was examined BV/TV (trabecular bone volume per total volume).[25,26]

Histological analysis (TRAP and H&E staining)

The fixed femur and tibia were immersed in 10% ethylene diamine tetraacetic acid (EDTA) for 4 weeks for decalcification and then embedded in paraffin to perform histological sections. The segments were examined by TRAP and H&E staining, using premium microscope known as Aperio Scanscope (Mt Waverley, VIC, Australia) to observe and photographed. The number of TRAP positive cells and osteoclasts surface or bone surface area (OCs/BS) of each field were calculated by ImageJ software (NIH, Bethesda, MD, USA).

Calcein-alizarin red S labeling and von Kossa staining

20 mg/kg calcein (Sigma-Aldrich, C0875-5g, 1 mg/mL in 2% NaHCO3 solution) and 40 mg/kg alizarin red S (Sigma-Aldrich, a5533-25g, 2 mg/mL in H_2O) were injected intraperitoneally on days 0 and 4, respectively. On day 7, the mice were sacrificed, the bones were fixed, dehydrated and embedded with embedded-812 (Electron Microscope Science). The samples were cut into 5 μm with a hard tissue cutter (RM2265, Leica, Wetzlar, Germany). Fluorescent labeling images were obtained with a microscope (BX51, Olympus).

For von Kossa staining, the femur samples were sliced into 6 μm dense pieces. Subsequently, the sections were irradiated with ultraviolet light in 2% silver nitrate solution for 1 h and then incubated with 5% sodium thiosulfate for 2 min. Finally, the staining results were observed by a Diplan light microscope (Leitz).

QUANTIFICATION AND STATISTICAL ANALYSIS

Utilizing Graphpad Prism 9 (Graphpad Software Inc., San Diego, CA, USA), the data were examined from triplicate experiments expressed as mean ± SEM. One-way or two-way ANOVA and Student's t test were used for comparison between groups and $p < 0.05$ was considered to indicate a statistically significant difference.